HAL
open science

Crystalline Molybdenum Oxide Thin-Films for Application as Interfacial Layers in Optoelectronic Devices

André Luis Fernandes Cauduro, Roberto dos Reis, Gong Chen, Andreas K. Schmid, Christophe Méthivier, Horst-Günter Rubahn, Léo Bossard-Giannesini, Hervé Cruguel, Nadine Witkowski, Morten Madsen

▶ To cite this version:

André Luis Fernandes Cauduro, Roberto dos Reis, Gong Chen, Andreas K. Schmid, Christophe Méthivier, et al.. Crystalline Molybdenum Oxide Thin-Films for Application as Interfacial Layers in Optoelectronic Devices. ACS Applied Materials & Interfaces, 2017, 9 (8), pp.7717-7724. 10.1021/acsami.6b14228 . hal-01464322

HAL Id: hal-01464322

https://hal.sorbonne-universite.fr/hal-01464322v1

Submitted on 10 Feb 2017

HAL is a multi-disciplinary open access archive for the deposit and dissemination of scientific research documents, whether they are published or not. The documents may come from teaching and research institutions in France or abroad, or from public or private research centers.

L'archive ouverte pluridisciplinaire **HAL**, est destinée au dépôt et à la diffusion de documents scientifiques de niveau recherche, publiés ou non, émanant des établissements d'enseignement et de recherche français ou étrangers, des laboratoires publics ou privés.

Crystalline Molybdenum Oxide Thin-Films for Application as Interfacial Layers in Optoelectronic Devices

André L. F. Cauduro[1,], Roberto dos Reis[2], Gong Chen[2], Andreas K. Schmid[2], Christophe Méthivier[3], Horst-Günter Rubahn[1], Léo Bossard-Giannesini[4], Hervé Cruguel[4], Nadine Witkowski[4], and Morten Madsen[1,**]*

[1] NanoSYD, University of Southern Denmark, Alsion 2, 6400-Sønderborg, Denmark

[2] National Center for Electron Microscopy, The Molecular Foundry, LBNL, Berkeley, CA, 94720, US

[3] Sorbonne Universités, UPMC Univ Paris 06, CNRS UMR 7197, Laboratoire de Réactivité de Surface (LRS), 4 place Jussieu, 75005 Paris, France

[4] Sorbonne Universités, UPMC Univ Paris 06, UMR CNRS 7588, Institut des Nanosciences de Paris (INSP), 4 place Jussieu, 75005 Paris, France

[*] Electronic mail: cauduro@mci.sdu.dk

[**] Electronic mail: madsen@mci.sdu.dk

Keywords: Reactive sputtering; single crystalline MoO_3 thin films; substoichiometric nanoaggregates; post-annealing; electronic properties of metal-oxide surfaces.

Abstract

The ability to control the interfacial properties in metal-oxide thin films through surface defect engineering is vital to fine tune their optoelectronic properties and thus their integration in novel optoelectronic devices. This is exemplified in photovoltaic devices based on organic, inorganic or hybrid technologies, where precise control of the charge transport properties through the interfacial layer is highly important for improving device performance. In this work, we study the effects of *in situ* annealing in nearly stoichiometric MoO_x (x~3.0) thin-films deposited by reactive sputtering. We report on a work function increase of almost 2 eV after inducing in situ crystallization of the films at 500°C, resulting in the formation of a single crystalline α-MoO_3 overlaid by substoichiometric and highly disordered nanoaggregates. The surface nanoaggregates possess various electronic properties, such as a work function ranging from 5.5 eV up to 6.2 eV, as determined from low-energy electron microscopy studies. The crystalline underlayer possesses a work function greater than 6.3 eV, up to 6.9 eV, characteristic of a very clean and nearly defect-free MoO_3. By combining electronic spectroscopies together with structural characterizations, this work addresses a novel method for tuning, and correlating, the optoelectronic properties and microstructure of device-relevant MoO_x layers.

1. INTRODUCTION

Transition metal-oxide (TMO) films like molybdenum oxide (MoO_x) have shown a variety of technological applications in the past years in the field of crystalline silicon (c-Si),[1,2] organic[3] and perovskite[4] solar cells. They are widely applied as hole extraction layers, facilitating low-resistance hole transport out of the absorber, *e.g.* in c-Si heterojunctions.[5] Furthermore, their usage has also been demonstrated to improve the stability of organic[6] and perovskite[7] solar cells, as well as of organic light emitting devices.[8] Other applications based on MoO_x films, such as gas and chemical sensors[9–11] and

storage devices such as memristive, memcapacitive[12] and Lithium-ion[13] devices were also reported recently.

All technological applications demonstrated in recent years, however, use mainly solution processed[14,15] or thermally evaporated[16,17] MoO_x as the fabrication method, which typically present a short-range-order structure (amorphous-like). Although there have been few reports addressing crystallization processes for these thin-films,[1,18–20] there has been a lack of studies addressing the impact of the crystallization of TMOs on the microstructure and electronic properties, which greatly affect their use in device applications. As an alternative deposition method, we have recently shown that by modifying the oxygen partial pressure during a DC-magnetron sputtering process, one can controllably tune the optoelectronic properties of as-deposited MoO_x[21] thin-films *via* defect engineering of oxygen vacancies (V_O), a technology that can even be further adopted to several other TMOs such as VO_x and WO_x. In this direction, Greiner *et al.*[22] have demonstrated how the work function and electronic states of transition metal-oxides are affected by induced defects or changes in the cation oxidation state, making them unique for a broad range of applications. However, sputtered MoO_x films typically possess short-range order, which potentially limits their use as transport or interfacial layers in devices. By having long-range-order TMO interfacial layers, one could improve the electrical charge transport at the interfaces (extraction/injection of carriers), which can be through delocalized states instead, *e.g.* by increasing both carrier mobility and carrier concentration in the films.[18,23] Therefore, a full understanding of the MoOx films microstructure and its correlation to the electronic properties is needed for improving its use in device applications.

In this work, we report on the crystallization of amorphous DC-sputtered MoO_x thin-films and correlate the nanoscale structure of the films to the electronic properties as well as to the surface morphology. Specifically, a phase transition to a crystalline orthorhombic MoO_3 underlayer structure with substoichiometric nanoaggregates on the surface of the film is observed. The surface composition of the film is assessed by X-ray photoelectron spectroscopy (XPS), while the occupied and unoccupied

bands are probed by ultraviolet photoelectron spectroscopy (UPS) and low-energy electron microscopy (LEEM), respectively, demonstrating the formation of the nanoscale substoichiometric domains over the stoichiometric MoO_3 phase. To the best of our knowledge, this is the first report on the correlation between the nanoscale structure of MoO_x and the electronic properties of the surface. This work shows an easy processable way of tuning and increasing the work function of MoO_x thin-films from a crystallization method, which is considered to be relevant for future device integration.

2. RESULTS AND DISCUSSIONS

2.1 Study of the valence band edge (UPS) and core level (XPS)

Figure 1 displays both the UPS and the XPS data and its analysis as a function of annealing temperature for MoO_x thin films prepared *ex situ* by DC-reactive sputtering. Figure 1a shows the secondary electron cut-off region of the 50 nm MoO_x thin-film as function of *in situ* annealing temperature under UHV conditions. A significant shift of the electron cut-off energy towards lower binding energies indicates an increase of the average work function (Φ) from 4.8 eV at room temperature up to 6.3 eV after annealing at 500°C. Φ values were calculated by extrapolating the linear part of the electron cut-off energy to zero intensity and by subtracting this energy from the photon energy (21.22 eV). Work function values versus annealing temperature are depicted in Figure 1b. For the first part of the thermal treatment under UHV (from room temperature up to 200°C), it has been previously reported that air exposed MoO_x thin-films are known to contain adsorbates such as moisture and carbon, which are responsible for lowering the work function of the as-deposited MoO_x films prepared from solution[14] or thermal evaporation.[24] Upon annealing of the contaminated films, however, Meyer *et al.*[14] and Irfan *et al.*[24] reported a work function recovery from 5.4 eV up to 6.0 eV at 200°C for 1 h and 5.4 eV up to 6.3 eV at 460°C for 30 min, respectively, where both studies indicate that this recovery process may take place *via* an upward shift of the vacuum level. Here, we report on a very

similar effect for post-annealed MoO_x deposited by DC reactive sputtering, especially up to 200°C. However, the work function value obtained at 500°C in this work, as it will be further discussed in the LEEM section, is much higher than in the studies reported earlier, *i.e.* an increase from 5.6 eV at 200°C to 6.3 eV at 500°C is observed by UPS, whereas domains with work function values up to 6.9 eV are evidenced by LEEM. As it will be discussed in the next section, the process of crystallization plays a crucial role on to the electronic properties of thin-films, and more precisely in the high work functions registered.

The UPS spectra, as a function of the annealing temperature showing the valence band edge of the region close to the Fermi level, are displayed in Figure 1c. A prominent peak centered at around ~1 eV, indicated by 'd' in Figure 1c, grows from RT up to 200°C, which is attributed to a change in occupancy of the Mo 4*d* band, *i.e.*, oxygen vacancy sites are created and thus modify the cation oxidation state of the neighboring molecules (it, *e.g.*, reduces from Mo^{+6} to Mo^{+5}) and, as a result, the electron occupancy of the 'd' band is increased.[25] As the electronic occupancy of the Mo 4*d* band increases, one expects an upward shift of the Fermi level that leads to a decreasing of the oxide work function.[22,26] In the case shown here and, as indicated by the electron cut-off energy shown in Figure 1a, surface adsorbates play a more significant role on the sample's work function at these low temperatures. But at the same time, despite the fact that the 'd' band increases with temperature, the surface of the sample gets cleaner, *i.e.* there is less carbon contamination on the surface (see Supplementary Figure S1) leading to an increase in work function from RT up to 200°C. However, when the annealing temperature reaches 500°C, a change in the valence spectrum edge is observed (see Figure 1c). The valence spectrum now extends up to the Fermi level, indicating a change in the character of the sample. The latter is no longer semiconductor at the surface, but it presents a metallic-like character instead (no band gap is evidence). Greiner *et al.*[27] have observed a similar behavior on *in-situ* oxidized Mo surfaces (deposited by sputtering). Starting from a nearly stoichiometric film, and followed by post-annealing at 250°C for 4 hours, a strong reduction of the surface and yet a high work function of nearly 6.00 eV have been

reported by XPS and UPS, where the core level analysis revealed the appearance of only two species, attributed to Mo^{+4} and Mo^{+5}.[27] In order to deeply understand the XPS and UPS analysis of the sample shown in Figure 1c, a further reduction of the surface has been performed (in a separate sample). As the Mo^{+5} and Mo^{+4} concentration raise on the surface, a clear metallic character is seen with a lower work function (~6.1 eV), and the valence band now resembles the one reported from Greiner *et al.* [27] (see Supplementary Figure S5 for UPS and Supplementary Figure S6 for XPS spectra). In order to go further in the understanding of the above observations, the XPS spectra, shown in Figure 1d, points out the presence of three different oxidation states on the clean surface of the sample (no carbon contamination has been quantified by XPS at 500°C, see Supplementary Figure S1). Thus, we evidence a formation of a very complex oxide here, formed by high-temperature annealing and composed of Mo^{+6}, Mo^{+5} and Mo^{+4} species in a ratio of 65.45%:27.12%:6.43% ,with binding energies of 232.50 eV, 231.60 eV and 229.70 eV, respectively. Table 1 summarizes the parameters extracted from the XPS analysis. The average oxidation states in Table 1 indicates a formation of a substoichiometric oxide even for the as-deposited films (RT) and its oxidation state value remains more-or-less unchanged up to 200°C, but it then decreases for the film formed at 500°C, which is explained by the appearance of the Mo^{+4} state at the surface, Figure 1d. As mentioned, the valence band edge shown in Figure 1c shows an intensity increase of the defect band from RT up to 200°C, corresponding to a reduction of the oxidation state, although the XPS indicates almost non-changing values in this range (slightly increasing here). The carbon contamination still present up to 200°C might screen the photoemitted electrons, and therefore a slight increase on the average oxidation state is observed up to 200°C.

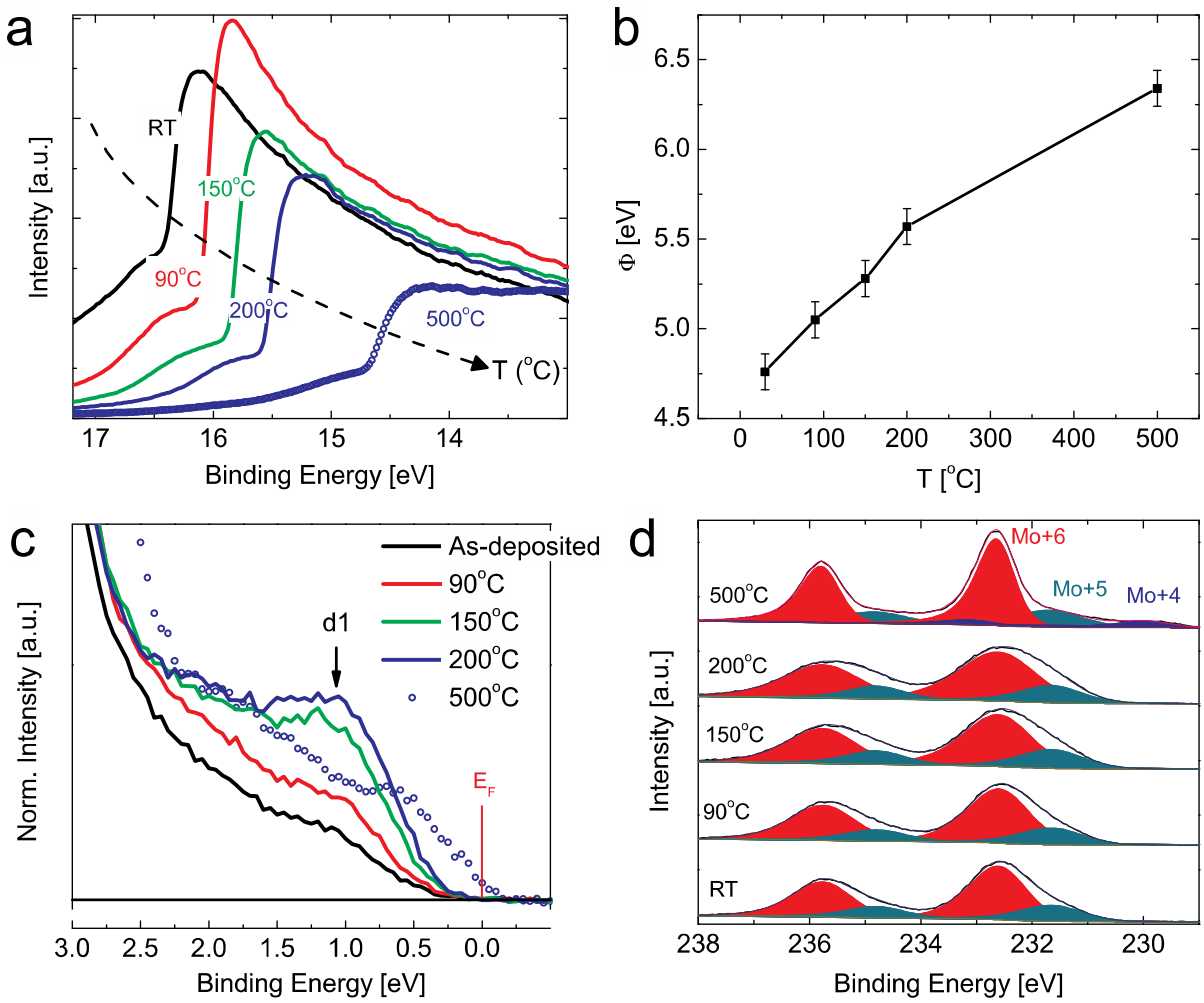

Figure 1. Photoemission analysis of the as-deposited and post-annealed MoO_x thin films. (a) Secondary electron cut-off energy. The tail of intensity at high binding energy originates from an artifact of the spectrometer. The dashed line is placed as a guide to the eye. (b) Work function extracted from the secondary electron cut-off as a function of annealing temperature. (c) 'd' indicates the defect band which is formed due to oxygen deficiency and which is depicted at ~1 eV near the E_F. The intensity of the defect band increases with temperature, reaching its maximum at 200°C. At 500°C the band occupancy extends up-to the Fermi level, changing the character of the surface to metallic-like instead. The black solid line indicates the zero intensity background level. (d) XPS spectra showing the surface chemistry evolution with temperature.

The inelastic mean free path is the major source of uncertainties in XPS, and it has been considered constant throughout the evaluation of the abundance of the elements (Mo, O and C). Interestingly, the spectral width (FWHM) of Mo^{+6} of the film formed at 500°C, which has been obtained by fitting the curves using asymmetric Gaussian-Lorentzian peaks, shows a decrease from 1.17 eV at RT down to

0.77 eV, being a strong evidence of structural changes within the film attributed to a better ordering in the layer (see Table 1).

Table 1. XPS fitting parameters and corresponding work function evaluated from UPS secondary electron cut-off.

T [°C]	Mo $3d_{5/2}$[a] Binding energy [eV] Peak area (%)			AVG[a] oxidation state	FWHM [eV][a] (+4/+5/+6)	Φ [eV][b]
	Mo^{+4}	Mo^{+5}	Mo^{+6}	-----	-----	-----
RT	-----	231.60eV (24.71%)	232.50eV (75.29%)	5.75	--/1.29/1.17	4.8
90°C	-----	231.60eV (24.18%)	232.50eV (75.82%)	5.76	--/1.30/1.27	5.1
150° C	-----	231.60eV (23.56%)	232.50eV (76.44%)	5.75	--/1.28/1.44	5.3
200° C	-----	231.60eV (22.29%)	232.50eV (77.71%)	5.78	--/1.28/1.58	5.6
500° C	229.70 eV (6.43%)	231.60eV (27.12%)	232.50eV (66.45%)	5.60	1.09/1.62/0.77	6.3

[a] Asymmetric Gaussian-Lorentzian peaks were used to fit all XPS spectra using Shirley background.

[b] Work function measurements were done by linear extrapolation of the electron cut-off region to zero energy and subtracting this value to the photon energy (21.22 eV).

2.2 Nanoscale structure of *in situ* annealed MoO_x films

Figure 2 shows AFM images of the MoO_X thin-films as a function of the annealing temperature. Clearly, the surface remains nearly unchanged up to 200°C, as depicted in Figure 2a and 2b. We have previously reported on DC-reactive sputtered MoO_x thin-films with very low surface roughness that present amorphous structure, independently of the oxygen partial pressure in the sputter regime of 10^{-3} mbar.[21] For the case of the film annealed at 500°C, on the other hand, the topology changes significantly and different domains appear on the surface. The surface nanoaggregates present different

adhesion properties as compared to the background of the sample being a first evidence that at least two distinct MoO_x phases are being formed at the surface as a result of the crystallization process (see Supplementary Figure S3). Figure 3 shows the structural and chemical analysis performed on the sample after flash annealing at 500°C. Cross sectional High-Resolution TEM (HRTEM) micrographs indeed demonstrate the formation of a highly crystalline sublayer (Figure 3a). Crystalline MoO_3 predominantly stabilizes as orthorhombic α-phase (Pbnm, Space Group #62) where edge and corner sharing MoO_6 octahedron are linked to create [010] stacked bilayer sheets. A magnified view of the top surface (blue boxed area in Figure 3a) clearly shows a transition from a high crystalline MoO_3 structure to a disordered, and presumably, substoichiometric region of about 40Å (Figure 3b). A close view from the middle region of the layer through the [010] direction projects the (100) planes with measured lattice space of 4.00(± 0.05) Å as indicated in Figure 3c. The Selected Area Diffraction (SAD) pattern in Figure 3d confirms the formation of α-MoO_3 structure. Some of the main diffraction spots corresponding to the substrate Si and the MoO_3 layer are highlighted with blue and white squared boxes, respectively. Blue boxes I, II and III correspond to the planes $(2\underline{2}0)$, $(1\underline{1}1)$ and (002), respectively, of the Si substrate viewed through the [011] zone axis. White boxed spots, Ia, IIa, and IIIa correspond to the (010), (021) and (100) planes, respectively. Despite the presence of an interfacial SiO_2 layer between the Si substrate and the deposited MoO_x layer, the crystallized structure formed through flash annealing at 500°C follows an epitaxial relationship $[002]_{Si}/[100]_{MoO3}$ with a slight misfit of about 2°.

Figure 3e and 3f show the High-Angle Annular Dark-Field (HAADF) survey image and chemical maps extracted by using Mo and O K-lines, respectively, obtained by EDX measurements under STEM mode. They demonstrate an overall compositional homogeneity throughout the MoO_3 layer at the resolution of 2.5 nm/pixel. The atomic percentage ratio of Mo:O is determined to be 1:3, quantified

based on the intensities of measured peaks of Kα-lines relative to calculated or measured intensities of standards.[28]

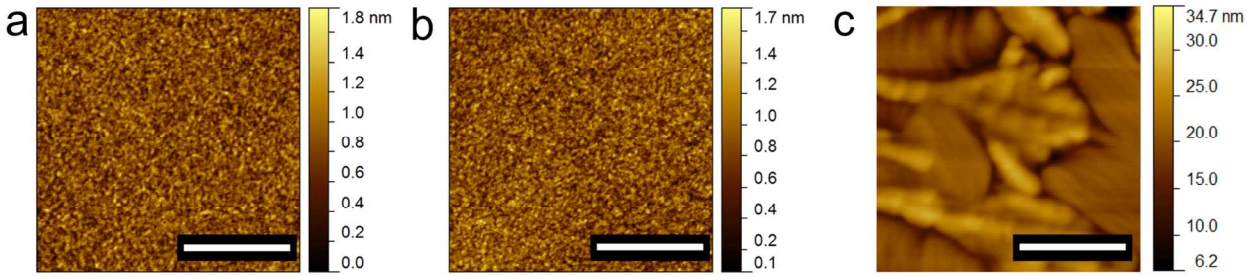

Figure 2. Atomic force microscopy of the MoOx thin films at different annealing temperatures. As-deposited (a), annealed at 200°C (b) and annealed at 500°C (c). Nanoaggregates appear on the surface for the case of flash annealing at 500°C under UHV conditions. The root mean square of the roughness is calculated as 4.21 nm. Scale bar is 400 nm.

It has been shown by Bhosle *et al.*[23] that MoO_x epitaxially grown on c-plane sapphire by pulsed laser deposition (PLD) leads to a monoclinic structure which is characteristic for the MoO_2 phase where the structure follows the growth along the (0001) direction, consisting of 60% of Mo^{+4}, 8.3% Mo^{+5} and 31.7% Mo^{+6}, according to XPS analysis. Their results also point out interesting optoelectronic properties such as very low electrical resistivity (7.2×10^{-5} Ω.cm) and high transparency (50%) for the as-deposited films. However, no phase transition was seen after a post-growth annealing, and the monoclinic structure remained unchanged. Modifications on the average oxidation state (Mo^{+6} increases up to 74%), on the resistivity (increases to 10^{-3} Ω.cm) and on the transparency (65%), nevertheless, were further observed for post-growth annealing under air atmosphere.[23] A similar work on the epitaxy of MoO_3 at variable temperature on c-sapphire from Koike *et al.* [29] demonstrated a formation of nearly single crystalline α-MoO_3 at a growth temperature of about 350°C. The disadvantage of their technique, however, is the fact that the epitaxy process is a non-feasible technique if one deposits over insulator substrates, which therefore might be a limiting factor for device integration. Sook Oh *et al.*[18] have shown a formation of polycrystalline MoO_x films *via* ultralow

pressure sputtering technique combined with post-annealing in argon ambient. In their results, the formation of longer range-order films has led to higher mobility (~40 $cm^2.V^{-1}.s^{-1}$) and higher carrier concentration (~10^{21} cm^{-3}). Here, we demonstrate a combination of a sputter deposition method along with annealing under UHV which generates a novel and nearly single crystalline MoO_x layer with very deep electronic states, where these characteristics could be an interesting route for implementation in state-of-art optoelectronic devices.

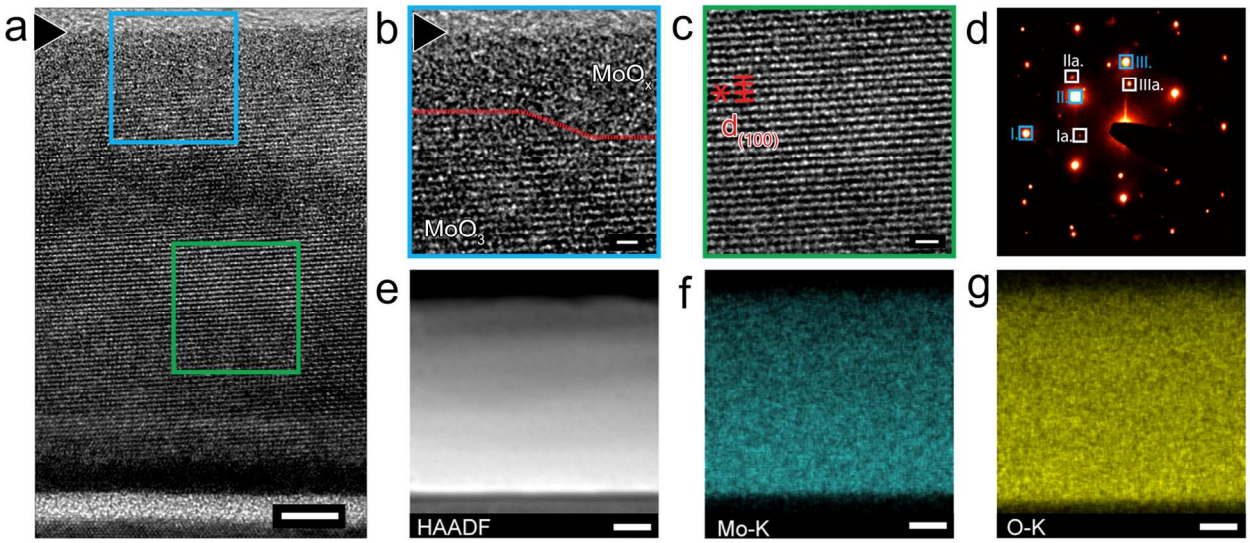

Figure 3. Microstructure characterization of sample after flash annealing at 500°C. (a) HRTEM micrograph showing the overall high crystallinity of MoO_3 throughout the layer (Scale bar of 5nm). (b) Shows a magnified view from the top surface within the blue box in (a). Red dotted line depicts the interface between crystalline layer to a disordered top surface. A magnified view of a region in the middle of the MoO_3 layer is shown in **(c)** with the (100) planes marked with red lines. (d) SAD pattern taken with the diffraction aperture covering both layer and substrate. White and blue squared boxes highlight some of the MoO_3 and Si substrate diffraction spots, respectively. **(e)** HAADF survey image alongside with 2-D EDX chemical maps produced by using (f) Mo K-Lines and (g) O-K-Lines atomic % intensity. Chemical maps demonstrate the layer homogeneity at the scale of 2.5 nm/pixel. Scale bar for (a) corresponds to 5nm, while for (b) and (c) to 0.1nm, and for (e)-(f) to 10nm. Arrowheads in (a), (b) and (e)-(f) indicate the top surface.

2.3 Study of the electronic properties and their correlation with the nanoscale structure

Bright-field LEEM images are formed from elastically reflected intensity of a coherent beam of low-energy electrons, which impinge normally on the surface of the specimen. The energy of the incident electrons, namely the landing energy E_0 of the electrons, can be varied. Thus LEEM gives spectroscopic- as well as microscopic information with high lateral resolution (~15 nm), being a very useful technique to study nanoscale electronic properties of materials, such as the work function. At a landing energy $E_0<0$, electrons are 100% reflected from the surface without interacting with it (mirror mode). At higher energy electrons are partly absorbed and partly reflected as a function of the unoccupied density of states at E_0 in the material.[30] This leads to a pronounced image intensity drop off as E_0 is swept from below- to above the work function. Sets of images recorded while sweeping E_0 represent pixel-by-pixel intensity-versus-voltage (I/V) curves that allow pixel-by-pixel measurement of the work function by mapping this intensity drop off. The bright-field image of the annealed sample (500°C) is shown in Figure 4a for E_0 = 6.0 eV and it reveals the formation of various nanostructures over the surface (see Supplementary Movie for full dataset). Figure 4b presents the two-dimensional map of the work function from the same area as shown in Figure 4a. The dark spots in Figure 4a correspond to areas with lower work function, which correlate to the rough structures seen by AFM in Figure 2c. The flat parts in between, the orange and yellow areas in Figure 4b, represent the high work function areas reaching from 6.3-6.7 eV. The formation of the substoichiometric oxide (with x<3), which happens quickly under UHV at high temperature, thus stands as the main explanation for the formation of the MoO_x nanoaggregates. Low-energy electron diffraction (LEED) indicates lack of crystalline structure on the top surface, *i.e.*, a surface composed by a more disordered and reduced MoO_x (Supplementary Figure S4.).

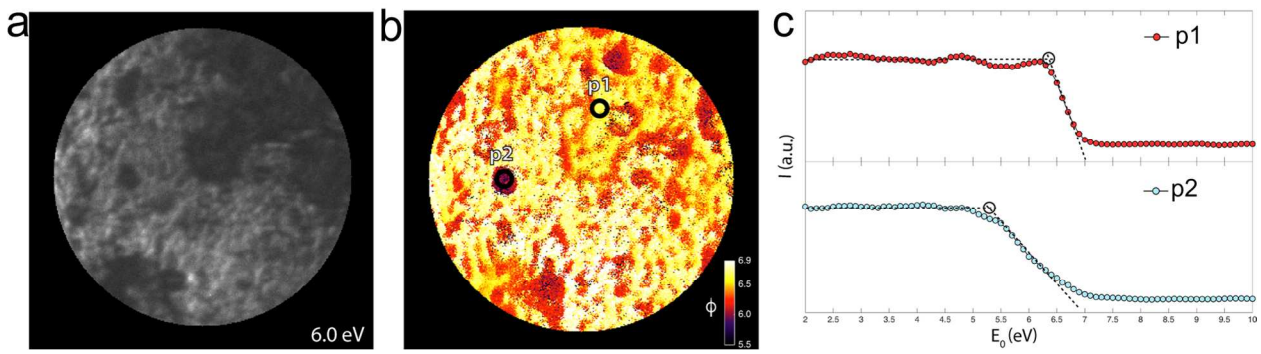

Figure 4. Low energy electron microscopy (LEEM) analysis. (a) LEEM image acquired at a landing energy of E_0 = 6.0 eV using 10.5 μm aperture. (b) Spatial map of work function in the same area. Color bar from 5.5 to 6.9eV (error within +/- 0.1 eV). (c) IV-curves extracted from two different points with distinct work functions indicated in panel b as p1=6.5 eV and p2=5.5 eV. Spectra were collected from single pixels.

Figure 4c shows the I-V curves from points "p1" and "p2" indicated in Figure 4b, which represent an area close to the stoichiometric MoO_3 and an area with O deficiency on the surface, respectively. The landing energy E_0 on which the intensity drops to zero is clearly shifted in both cases, corresponding to the different work function values.

3. SUMMARY AND CONCLUSION

In this work, the formation of crystalline MoO_3 from an amorphous MoO_x sputtered thin-film is demonstrated. Detailed investigations of the films show large changes in the surface chemistry, the occupied and unoccupied states and the work function from XPS, UPS and LEEM studies, respectively, and are discussed below. This combined experimental work represents the main research findings and is presented in Figure 5:

1) A phase transition from a non-crystalline solid to an orthorhombic α-MoO_3 underlayer bulk-film is demonstrated. We propose a novel crystallization method that generates a very clean surface with an average high work function of around 6.3 eV (being close to *in situ* prepared, nearly stoichiometric MoO_3 films, having work functions up to 6.9 eV).[16] Figure 5a represents the highly disordered MoO_x

film, which remains nearly unchanged up to 200°C, while Figure 5c represents the single crystalline MoO_3 sublayer structure along with the work function of the surface measured by LEEM (yellow arrow pointing to the work function color bar), obtained at 500°C. To the best of our knowledge, this is the first report on the correlation between the nanoscale structure of MoO_x and the electronic properties of the surface.

2) Generation of surface nanoaggregates (MoO_x) that hold different electronic properties than the MoO_3 crystalline bulk is presented. A very complex MoO_x surface composed of at least 2 different stoichiometries (x~3.0 and x<3.0) is seen by LEEM studies, from where it is possible to determine nanoscale regions with work function of about 5.5-6.2 eV, corresponding to highly reduced MoO_x (x<3), and regions where the work function is greater than 6.3 eV (up to 6.9 eV), corresponding to crystalline MoO_3 (see Figure 5c). The LEEM results are in accordance with the XPS and UPS studies, which have shown the presence of Mo^{+4} and a substantial change of the DOS near the valance-band edge, indicating a metallic-oxide character of the surface (Figure 1b and 1c and Figure 5d).

In conclusion, we have shown a detailed experimental protocol for developing MoO_x thin-films with specific microstructure and electronic properties using a reactive sputtering technique combined with post-fabrication UHV annealing. The films possess very high work function and also a highly ordered sublayer structure, properties that combined are very important for hole selective layers *e.g.* in crystalline-silicon c-Si, organic and hybrid photovoltaics. It is also expected that the films formed at 500°C possess higher conductivity at the surface (due to the formation of the metallic-like MoO_x nanoaggregates) and higher carrier mobility due to formation of the single crystalline α-MoO_3.

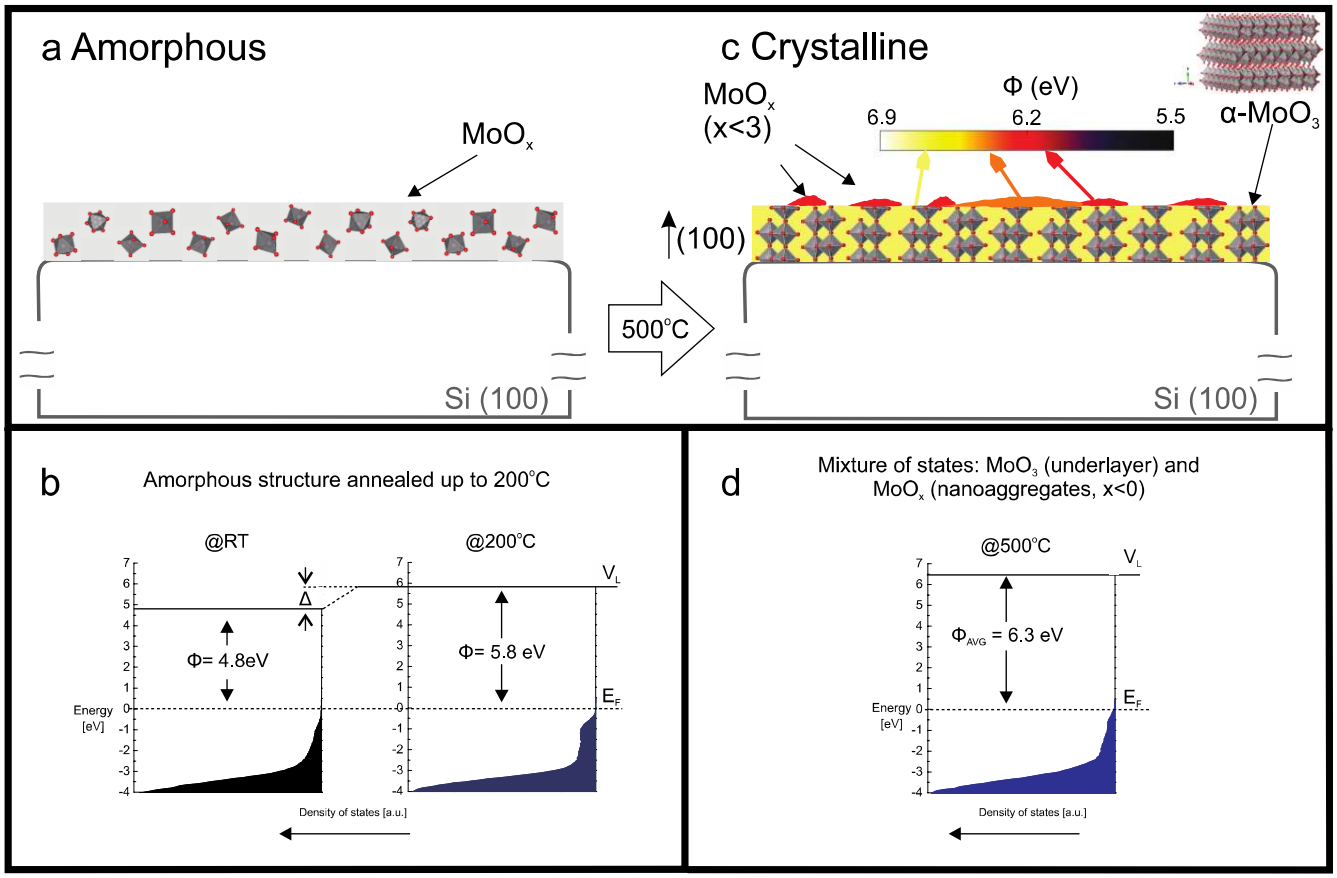

Figure 5. Schematic diagram representing the phase transition and the energy band of the crystalline MoO_3 structure formed at 500°C vs. the amorphous MoO_x structure present up to 200°C. (a) Amorphous MoO_X in detail represented by randomly placed octahedral within the film. Each octahedron is formed by one Mo atom, which is surrounded by six octahedrally coordinated O atoms. (b) Energy diagram of the amorphous structure from RT and after post-annealing at 200°C representing the work function change *via* an upward shift of the vacuum level (VL) as indicated by Δ. The density of states (DOS) close to the Fermi level (E_F) increases with temperature, which is due to the formation of V_O. (c) Crystalline α-MoO_3 underlayer represented by the octahedral stacked along to a (100) direction formed after annealing of the structure shown in (a) at 500°C under UHV. A 3D view of the crystalline structure is detailed in the upper right corner. The a lattice plane has been measured to be a_{exp}= 4.00 Å (±0.05Å), which is in good agreement with the theoretical value (a_{theo}= 3.96 Å) extracted from the crystalline model. The MoO_x (x<0) overlayer is represented by the surface nanoaggregates holding different electronic properties (color bar indicates the work function at the nanoscale). (d) Energy-level diagram of the structure described in (c). It comprehends a mixture of states (orthorhombic MoO_3 in addition to the nanoaggregate MoO_x with different composition). A higher DOS close to the E_F indicates an absence of transport gap, which is a characteristic of highly reduced metallic oxides. The DOS near the valance band edge is plotted from the UPS spectra as it stands as a fairly good first approximation.

4. EXPERIMENTAL SECTION

Nearly stoichiometric MoO_x thin-films (~50 nm) were deposited by using DC-reactive sputtering on highly doped n-type Si wafers (0.001-0.005 ohm.cm) under an oxygen partial pressure of ~$1.37x10^{-3}$ mbar and an argon partial pressure of $1.44x10^{-3}$ mbar[21]. The as-deposited films were exposed to the environment and then transferred into an ultrahigh vacuum (UHV) chamber with a base pressure of $5x10^{-10}$ mbar, where both ultraviolet photoelectron spectroscopy (UPS) and X-ray photoelectron spectroscopy (XPS) were carried out on a SPECS PHOIBOS 100-1DLD photoelectron spectrometer. UPS analysis was done using a He I (h□=21.22 eV) discharge lamp as the excitation source at $2x10^{-7}$ mbar, while XPS was conducted at $5x10^{-10}$ mbar using a monochromatic Al K_α source (h□=1486.7 eV). The spectrometer was calibrated using the Ag $3d_{5/2}$ peak at 368.21 eV and the Ag $3d_{3/2}$ peak at 374.21 eV after sputter cleaning the surface. Work function and valence-band measurements were done using UPS with the sample surface normal to the analyzer electrostatic lenses axis and under an applied bias of -10 V for the work function. *In situ* post-annealing experiments were conducted followed by further XPS/UPS experiments. The samples were annealed for 30 min at 90°C, 30 min at 150°C and 30 min at 200°C. The temperature measurements are within +-10° C. Additionally, a flash annealing was performed at 500°C for 5 min. XPS and UPS spectra were recorded following each step after sample cool down to about ~40°C. Transmission Electron Microscopy (TEM) and Scanning TEM experiments were performed by using a FEI Titan microscope operating at 200 kV. Standard cross-section thin foils was prepared from a sample annealed at 500°C by mechanical thinning and dimpling followed by Ar^+ ion polishing using a Gatan Precision Ion Polishing System operated at 3.0 keV with a 6° milling angle. A final polish using 0.5 keV at shallow angles (2°) was performed before the samples were analyzed. Conventional TEM micrographs were acquired with a Gatan UltraScan 1000 (2k x 2k) camera, while SAD patterns were recorded using a Gatan Orius 830 (2k x 2k). For STEM images, the scattered electrons were captured by a Fischione Model 3000 ADF detector. Energy Dispersive X-Ray (EDX)

spectra were collected for about 10 minutes by using a FEI SuperX quad windowless detector based on silicon drift technology with a solid angle of 0.7 steradian. LEEM experiments were performed in the spin-polarized LEEM system at the National Center for Electron Microscopy, Molecular Foundry at Lawrence Berkeley National Laboratory[31]. The MoO_x samples were flashed to 500°C for 5 minutes to clean the sample surface under ultrahigh vacuum. The energy resolution of the incident electrons is 0.1eV. The surface roughness was investigated by Atomic Force Microscopy (AFM) in tapping mode (Veeco Dimension 3100), while the mechanical properties of the surface were studied in Peak-Force mode of the AFM (Bruker Multimode 8) where the peak interaction force is used as a feedback control of the signal. During imaging, the force-curve (force vs. distance) for each point is recorded and used to display the mechanical properties of the surface.

ASSOCIATED CONTENT

Supporting Information

The supplementary information contains additional results that support the main research findings within the article (mechanical properties of the surface, XPS and LEED), explained in the supplementary note #1. The supplementary material also contains detailed information about the density of the filled states near the Fermi level and core level analysis by UPS and XPS, respectively, of a MoO_x surface that has been further reduced (x~2.6). This demonstrates formation of a valence band spectrum that resembles the one from MoO_2 (please see supplementary note #2).

Supplementary Movie: Full dataset of bright-field LEEM images that were used to evaluate the work function map displayed in Figure 2b.

The supporting information is available free of charge on the ACS Publications website at http://pubs.acs.org.

AUTHOR INFORMATION

Corresponding Author

* Electronic mail: cauduro@mci.sdu.dk

** Electronic mail: madsen@mci.sdu.dk

Notes

The authors declare no competing financial interest.

Author Contributions

A.L.F.C. and M.M conceived the idea and designed the experiments. A.L.F.C., C.M. and N.W. carried out XPS/UPS experiments and data analysis. R.R., G.C. and A.K.S. performed LEEM measurements and data analysis. R.R. contributed to TEM sample preparation, measurement and data analysis. A.L.F.C., L.B-G. and H.C. carried out AFM measurements and data analysis. All authors contributed to discussing the results and writing the manuscript.

ACKNOWLEDGEMENT

A.L.F.C. thanks the CNPq Brazilian Council for providing a scholarship under Process no 213909/2012-0. Work at the Molecular Foundry was supported by the Office of Science, Office of Basic Energy Sciences, of the U.S. Department of Energy under Contract No. DE-AC02-05CH11231. The research leading to these results has received funding from the People Programme (Marie Curie Actions) of the European Union's Seventh Framework Programme FP7/ 2007-2013/under REA Grant Agreement No. 607232, THINFACE.

REFERENCES

(1) Battaglia, C.; Yin, X.; Zheng, M.; Sharp, I. D.; Chen, T.; McDonnell, S.; Azcatl, A.; Carraro, C.; Ma, B.; Maboudian, R.; Wallace, R. M.; Javey, A. Hole Selective MoOx Contact for Silicon Solar Cells. *Nano Lett.* **2014**, 14, 967–971.

(2) Bullock, J.; Hettick, M.; Geissbühler, J.; Ong, A. J.; Allen, T.; Sutter-Fella, C. M.; Chen, T.; Ota, H.; Schaler, E. W.; De Wolf, S.; Ballif, C.; Cuevas, A.; Javey, A. Efficient Silicon Solar Cells with Dopant-Free Asymmetric Heterocontacts. *Nat. Energy* **2016**, 1, 15031.

(3) Vasilopoulou, M.; Douvas, A. M.; Georgiadou, D. G.; Palilis, L. C.; Kennou, S.; Sygellou, L.; Soultati, A.; Kostis, I.; Papadimitropoulos, G.; Davazoglou, D.; Argitis, P. The Influence of Hydrogenation and Oxygen Vacancies on Molybdenum Oxides Work Function and Gap States for Application in Organic Optoelectronics. *J. Am. Chem. Soc.* **2012**, 134, 16178–16187.

(4) Zhao, Y.; Nardes, A. M.; Zhu, K. Effective Hole Extraction Using MoOx-Al Contact in Perovskite CH3NH3PbI3 Solar Cells. *Appl. Phys. Lett.* **2014**, 104, 213906.

(5) Bullock, J.; Cuevas, A.; Allen, T.; Battaglia, C. Molybdenum Oxide MoOx: A Versatile Hole Contact for Silicon Solar Cells. *Appl. Phys. Lett.* **2014**, 105, 232109.

(6) Elumalai, N. K.; Saha, A.; Vijila, C.; Jose, R.; Jie, Z.; Ramakrishna, S. Enhancing the Stability of Polymer Solar Cells by Improving the Conductivity of the Nanostructured MoO3 Hole-Transport Layer. *Phys. Chem. Chem. Phys.* **2013**, 15, 6831–6841.

(7) Sanehira, E. M.; Tremolet de Villers, B. J.; Schulz, P.; Reese, M. O.; Ferrere, S.; Zhu, K.; Lin, L. Y.; Berry, J. J.; Luther, J. M. Influence of Electrode Interfaces on the Stability of Perovskite Solar Cells: Reduced Degradation Using MoO X /Al for Hole Collection. *ACS Energy Lett.* **2016**, 1, 38–45.

(8) Wang, F.; Qiao, X.; Xiong, T.; Ma, D. The Role of Molybdenum Oxide as Anode Interfacial Modification in the Improvement of Efficiency and Stability in Organic Light-Emitting Diodes. *Org. Electron.* **2008**, 9, 985–993.

(9) Di Giulio, M.; Manno, D.; Micocci, G.; Serra, a.; Tepore, a. Physical Properties of Molybdenum Oxide Thin Films for NO Gas Detection. *Phys. Status Solidi* **1998**, 168, 249–256.

(10) Alsaif, M. M. Y. a.; Field, M. R.; Murdoch, B. J.; Daeneke, T.; Latham, K.; Chrimes, A. F.; Zoolfakar, A. S.; Russo, S. P.; Ou, J. Z.; Kalantar-zadeh, K. Substoichiometric Two-Dimensional Molybdenum Oxide Flakes: A Plasmonic Gas Sensing Platform. *Nanoscale* **2014**, 6, 12780–12791.

(11) Eranna, G.; Joshi, B. C.; Runthala, D. P.; Gupta, R. P. Oxide Materials for Development of Integrated Gas Sensors—A Comprehensive Review. *Crit. Rev. Solid State Mater. Sci.* **2004**, 29, 111–188.

(12) Bessonov, A. A.; Kirikova, M. N.; Petukhov, D. I.; Allen, M.; Ryhänen, T.; Bailey, M. J. A. Layered Memristive and Memcapacitive Switches for Printable Electronics. *Nat. Mater.* **2014**, 14, 199–204.

(13) Chen, W.; Zhang, H.; Wang, Y.; Ma, Z.; Li, Z. In-Situ Microstructural Investigations by Electron-Beam Irradiation Induced Crystallization of Amorphous MoOx Thin Films with High Performance for Li-Ion Storage. *Electrochim. Acta* **2014**, 144, 369–375.

(14) Meyer, J.; Khalandovsky, R.; Görrn, P.; Kahn, A. MoO3 Films Spin-Coated from a Nanoparticle Suspension for Efficient Hole-Injection in Organic Electronics. *Adv. Mater.* **2011**, 23, 70–73.

(15) Girotto, C.; Voroshazi, E.; Cheyns, D.; Heremans, P.; Rand, B. P. Solution-Processed MoO 3 Thin Films As a Hole-Injection Layer for Organic Solar Cells. *ACS Appl. Mater. Interfaces* **2011**, 3, 3244–3247.

(16) Meyer, J.; Hamwi, S.; Kröger, M.; Kowalsky, W.; Riedl, T.; Kahn, A. Transition Metal Oxides for Organic Electronics: Energetics, Device Physics and Applications. *Adv. Mater.* **2012**, 24, 5408–5427.

(17) Matsushima, T.; Kinoshita, Y.; Murata, H. Formation of Ohmic Hole Injection by Inserting an Ultrathin Layer of Molybdenum Trioxide between Indium Tin Oxide and Organic Hole-Transporting Layers. *Appl. Phys. Lett.* **2007**, 91, 253504.

(18) Sook Oh, M.; Seob Yang, B.; Ho Lee, J.; Ha Oh, S.; Soo Lee, U.; Jang Kim, Y.; Joon Kim, H.; Soo Huh, M. Improvement of Electrical and Optical Properties of Molybdenum Oxide Thin Films by Ultralow Pressure Sputtering Method. *J. Vac. Sci. Technol. A Vacuum, Surfaces, Film.* **2012**, 30, 31501.

(19) Sian, T. S.; Reddy, G. B. Optical, Structural and Photoelectron Spectroscopic Studies on Amorphous and Crystalline Molybdenum Oxide Thin Films. *Sol. Energy Mater. Sol. Cells* **2004**, 82, 375–386.

(20) Lin, S. Y.; Wang, C. M.; Kao, K. S.; Chen, Y. C.; Liu, C. C. Electrochromic Properties of MoO3 Thin Films Derived by a Sol-Gel Process. *J. Sol-Gel Sci. Technol.* **2010**, 53, 51–58.

(21) Fernandes Cauduro, A. L.; Fabrim, Z. E.; Ahmadpour, M.; Fichtner, P. F. P.; Hassing, S.; Rubahn, H.; Madsen, M. Tuning the Optoelectronic Properties of Amorphous MoOx Films by Reactive Sputtering. *Appl. Phys. Lett.* **2015**, 106, 202101.

(22) Greiner, M. T.; Helander, M. G.; Tang, W.-M.; Wang, Z.-B.; Qiu, J.; Lu, Z.-H. Universal Energy-Level Alignment of Molecules on Metal Oxides. *Nat. Mater.* **2012**, 11, 76–81.

(23) Bhosle, V.; Tiwari, A.; Narayan, J. Epitaxial Growth and Properties of MoO[sub x](2<x<2.75) Films. *J. Appl. Phys.* **2005**, 97, 83539.

(24) Irfan, I.; James Turinske, A.; Bao, Z.; Gao, Y. Work Function Recovery of Air Exposed Molybdenum Oxide Thin Films. *Appl. Phys. Lett.* **2012**, 101.

(25) Greiner, M. T.; Chai, L.; Helander, M. G.; Tang, W. M.; Lu, Z. H. Transition Metal Oxide Work Functions: The Influence of Cation Oxidation State and Oxygen Vacancies. *Adv. Funct. Mater.* **2012**, 22, 4557–4568.

(26) Greiner, M. T.; Lu, Z.-H. Thin-Film Metal Oxides in Organic Semiconductor Devices: Their Electronic Structures, Work Functions and Interfaces. *NPG Asia Mater.* **2013**, 5, e55.

(27) Greiner, M. T.; Helander, M. G.; Wang, Z. B.; Tang, W. M.; Qiu, J.; Lu, Z. H. A Metallic Molybdenum Suboxide Buffer Layer for Organic Electronic Devices. *Appl. Phys. Lett.* **2010**, 96, 213302.

(28) Cliff, G.; Lorimer, G. W. The Quantitive Analysis of Thin Specimens. *J. Microsc.* **1974**, 103, 203–207.

(29) Koike, K.; Wada, R.; Yagi, S.; Harada, Y.; Sasa, S.; Yano, M. Characteristics of MoO 3 Films Grown by Molecular Beam Epitaxy. *Jpn. J. Appl. Phys.* **2014**, 53, 05FJ02.

(30) Jobst, J.; Kautz, J.; Geelen, D.; Tromp, R. M.; van der Molen, S. J. Nanoscale Measurements of Unoccupied Band Dispersion in Few-Layer Graphene. *Nat. Commun.* **2015**, 6, 8926.

(31) National Center for Electron Microscopy, Lawrence Berkeley National Laboratory, Berkeley, CA, U. S. National Center for Electron Microscopy, Lawrence Berkeley National Laboratory, Berkeley, CA, United States.

TOC

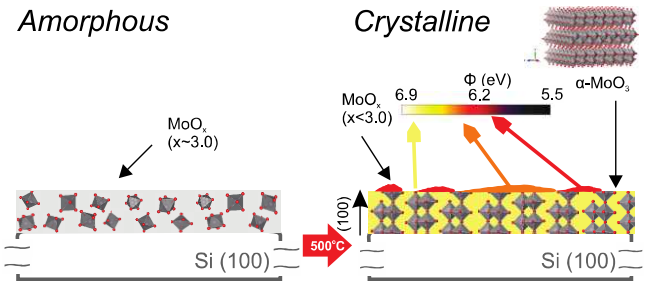

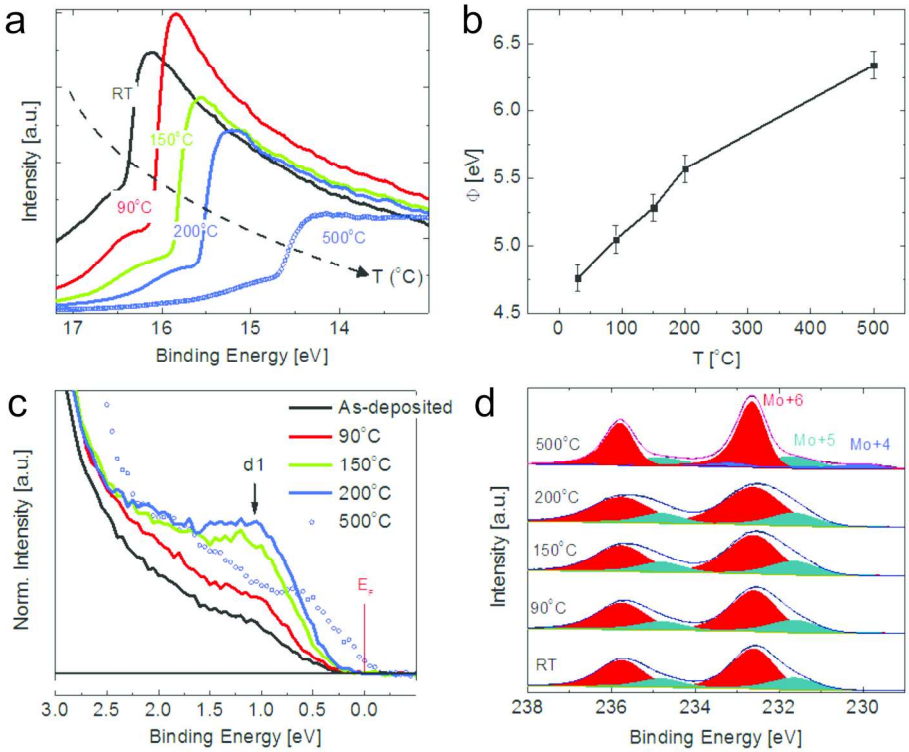

Figure 1. Photoemission analysis of the as-deposited and post-annealed MoOx thin films. (a) Secondary electron cut-off energy. The tail of intensity at high binding energy originates from an artifact of the spectrometer. The dashed line is placed as a guide to the eye. (b) Work function extracted from the secondary electron cut-off as a function of annealing temperature. (c) 'd' indicates the defect band which is formed due to oxygen deficiency and which is depicted at ~1 eV near the EF. The intensity of the defect band increases with temperature, reaching its maximum at 200°C. At 500oC the band occupancy extends up-to the Fermi level, changing the character of the surface to metallic-like instead. The black solid line indicates the zero intensity background level. (d) XPS spectra showing the surface chemistry evolution with temperature.

180x141mm (300 x 300 DPI)

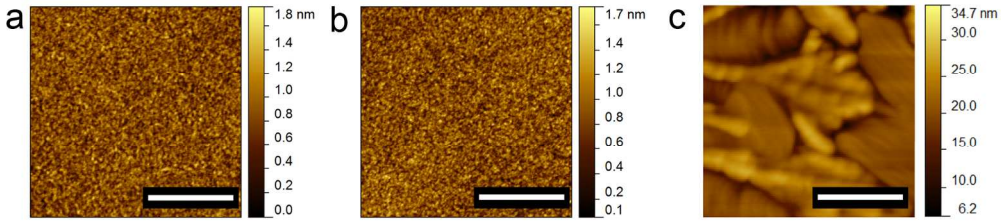

Figure 2. Atomic force microscopy of the MoOx thin films at different annealing temperatures. As-deposited (a), annealed at 200°C (b) and annealed at 500°C (c). Nanoaggregates appear on the surface for the case of flash annealing at 500°C under UHV conditions. The root mean square of the roughness is calculated as 4.21 nm. Scale bar is 400 nm.

180x39mm (300 x 300 DPI)

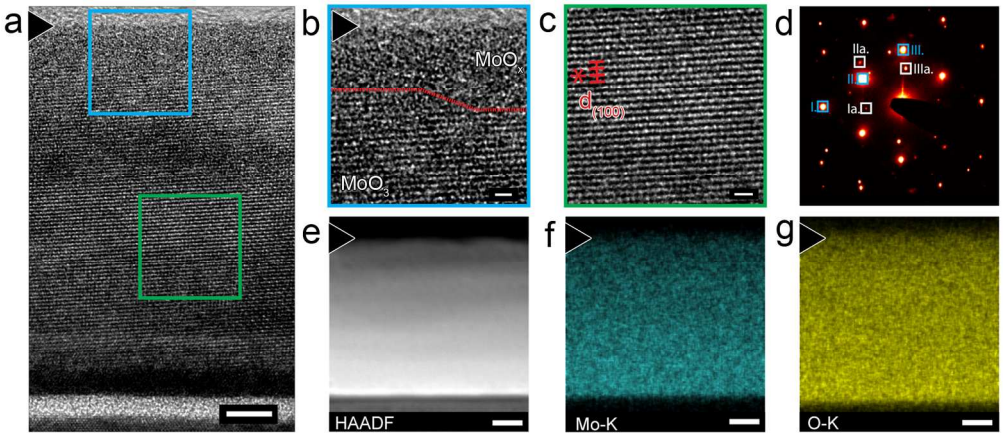

Figure 3. Microstructure characterization of sample after flash annealing at 500oC. (a) HRTEM micrograph showing the overall high crystallinity of MoO3 throughout the layer (Scale bar of 5nm). (b) Shows a magnified view from the top surface within the blue box in (a). Red dotted line depicts the interface between crystalline layer to a disordered top surface. A magnified view of a region in the middle of the MoO3 layer is shown in (c) with the (100) planes marked with red lines. (d) SAD pattern taken with the diffraction aperture covering both layer and substrate. White and blue squared boxes highlight some of the MoO3 and Si substrate diffraction spots, respectively. (e) HAADF survey image alongside with 2-D EDX chemical maps produced by using (f) Mo K-Lines and (g) O-K-Lines atomic % intensity. Chemical maps demonstrate the layer homogeneity at the scale of 2.5 nm/pixel. Scale bar for (a) corresponds to 5nm, while for (b) and (c) to 0.1nm, and for (e)-(f) to 10nm. Arrowheads in (a), (b) and (e)-(f) indicate the top surface.

180x78mm (300 x 300 DPI)

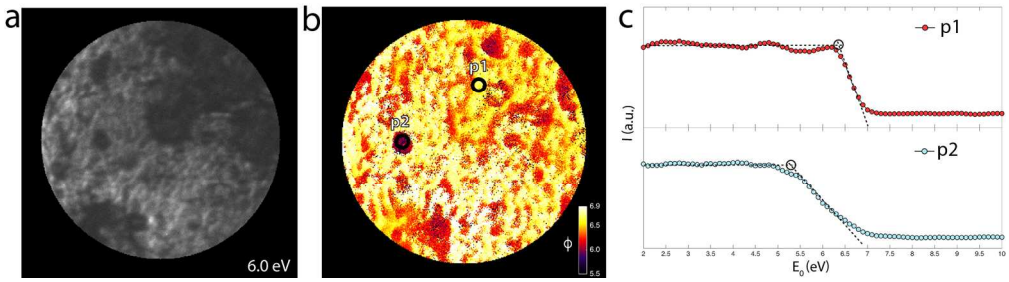

¬Figure 4. Low energy electron microscopy (LEEM) analysis. (a) LEEM image acquired at a landing energy of E0 = 6.0 eV using 10.5 μm aperture. (b) Spatial map of work function in the same area. Color bar from 5.5 to 6.9eV (error within +/- 0.1 eV). (c) IV-curves extracted from two different points with distinct work functions indicated in panel b as p1=6.5 eV and p2=5.5 eV. Spectra were collected from single pixels.

180x50mm (300 x 300 DPI)

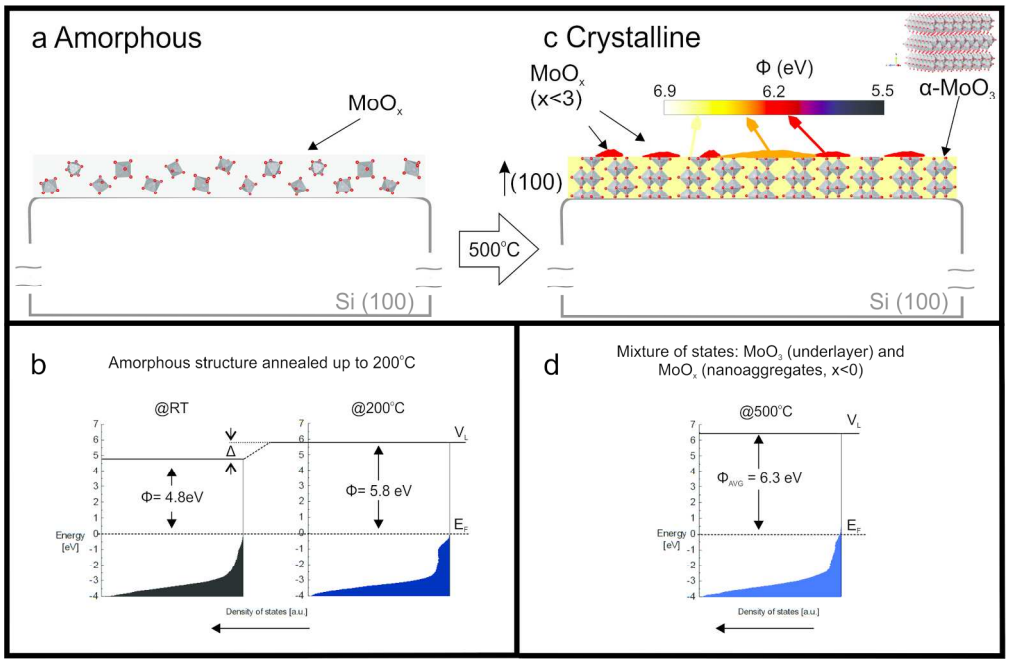

Figure 5. Schematic diagram representing the phase transition and the energy band of the crystalline MoO3 structure formed at 500°C vs. the amorphous MoOx structure present up to 200°C. (a) Amorphous MoOX in detail represented by randomly placed octahedral within the film. Each octahedron is formed by one Mo atom, which is surrounded by six octahedrally coordinated O atoms. (b) Energy diagram of the amorphous structure from RT and after post-annealing at 200oC representing the work function change via an upward shift of the vacuum level (VL) as indicated by Δ. The density of states (DOS) close to the Fermi level (EF) increases with temperature, which is due to the formation of VO. (c) Crystalline α-MoO3 underlayer represented by the octahedral stacked along to a (100) direction formed after annealing of the structure shown in (a) at 500°C under UHV. A 3D view of the crystalline structure is detailed in the upper right corner. The a lattice plane has been measured to be aexp= 4.00 Å (±0.05Å), which is in good agreement with the theoretical value (atheo= 3.96 Å) extracted from the crystalline model. The MoOx (x<0) overlayer is represented by the surface nanoaggregates holding different electronic properties (color bar indicates the work function at the nanoscale). (d) Energy-level diagram of the structure described in (c). It comprehends a mixture of states (orthorhombic MoO3 in addition to the nanoaggregate MoOx with different composition). A higher DOS close to the EF indicates an absence of transport gap, which is a characteristic of highly reduced metallic oxides. The DOS near the valance band edge is plotted from the UPS spectra as it stands as a fairly good first approximation.

181x118mm (300 x 300 DPI)